MODELING SELECTED SPECTRAL STATES OF 3C 279

K. NALEWAJKO (COPERNICUS), M. SIKORA (COPERNICUS), M. HAYASHIDA (SLAC/KIPAC AND KYOTO) AND G. M. MADEJSKI (SLAC/KIPAC)

We present models of three spectral states of blazar 3C 279 selected from an extensive multiwavelength campaign led by the Fermi Collaboration in years 2008-2010. We focus our attention on the February 2009 state (Period D), corresponding to the peak of gamma-ray and optical flares simultaneous with a polarization swing. Data from the Spitzer/MIPS indicate a sharp mid-IR spectral break, which can be explained either by a break in the electron energy distribution or by the synchrotron self-absorption. A transition between the spectral states at periods D and E, 15 days later, can be explained in the single blob propagation scenario at distances where external radiation is dominated by the infrared component. The flaring state can also be produced within the broad-line region, however an additional emission produced at larger distances is required to explain the millimeter and X-ray fluxes.

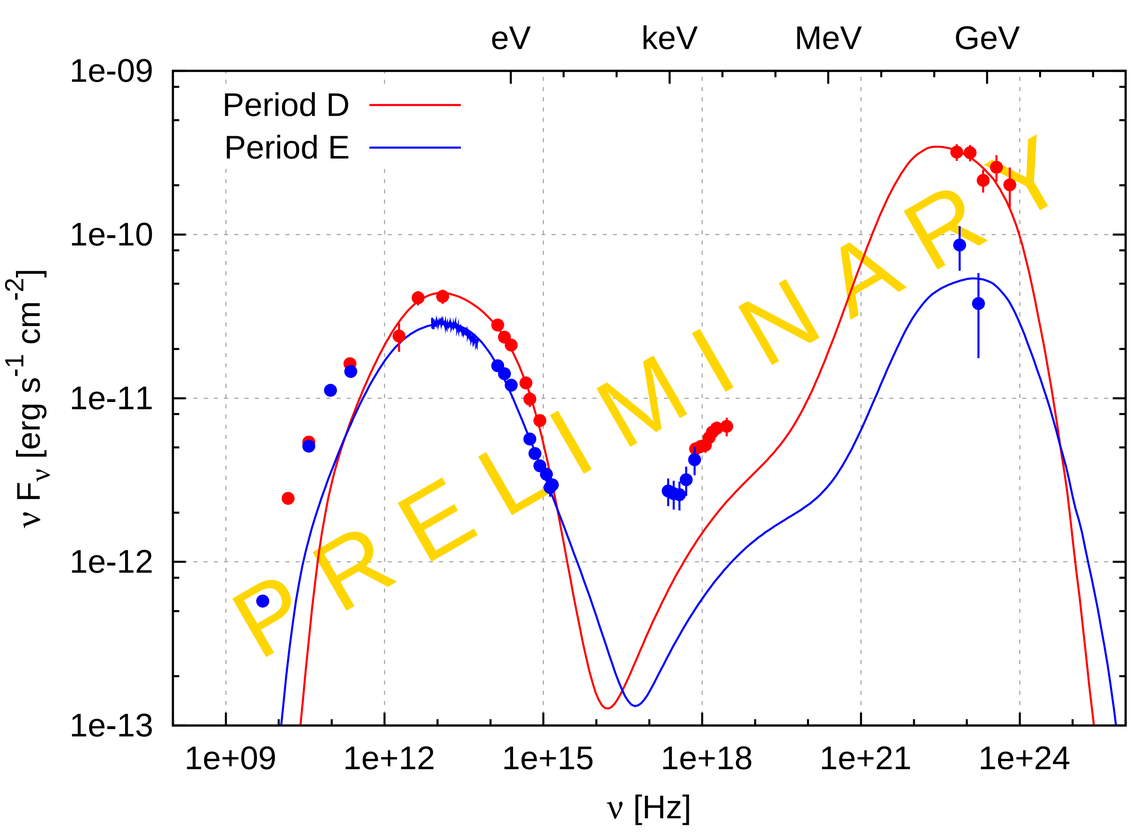

Figure 1: Spectral energy distributions of 3C 279 for Period D (MJD 54880-5; red) and Period E (MJD 54897-900; blue). Emission models D1 (red line) and E1 (blue line), dominated by the ERCIR components, assume source locations r and viewing angles $\theta_{\rm obs}$ consistent with propagation of a single blob on a curved trajectory.

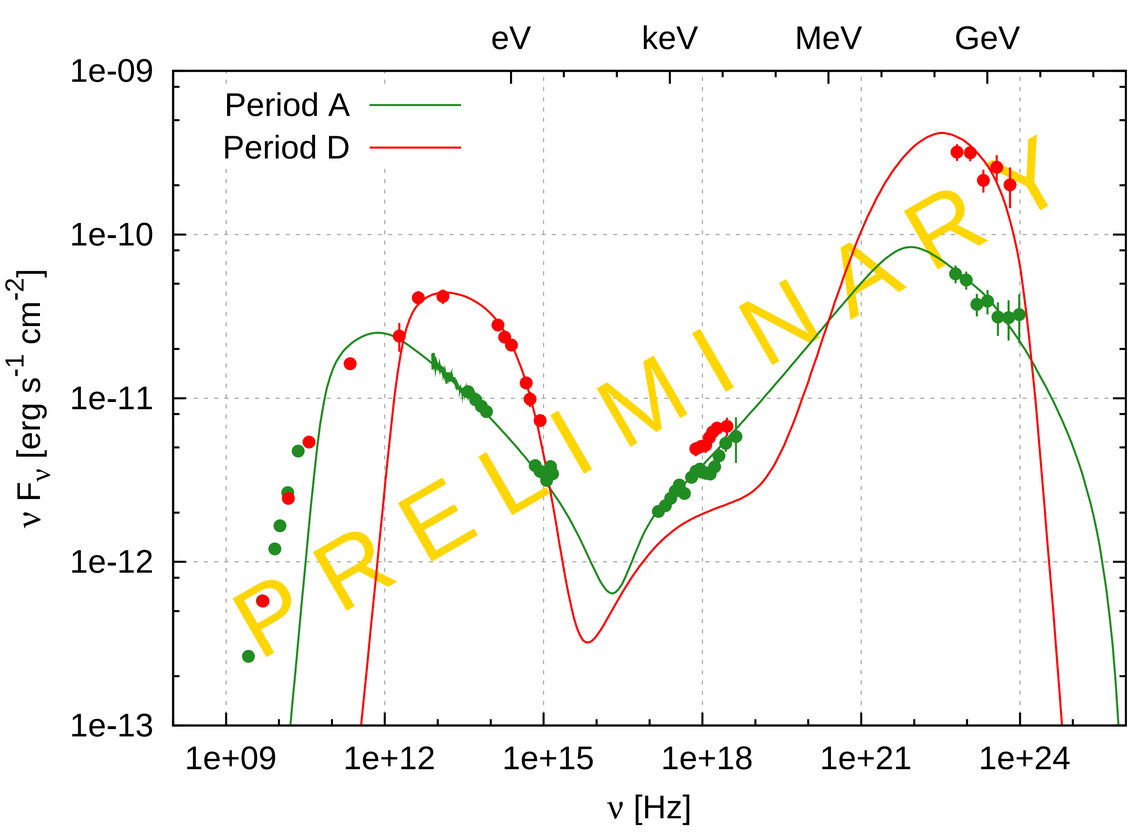

Figure 2: Spectral energy distributions of 3C 279 for Period A (MJD 54682-728; green) and Period D (MJD 54880-5; red). Model D2 (red line), dominated by the ERCBEL component, has the Spitzer/MIPS break explained with the synchrotron self-absorption. Model A2 (green line) is dominated by the ERCIR component.

3C 279 is a prominent Flat-Spectrum Radio Quasar located at redshift $z = 0.536$. It has been a target of an extensive multiwavelength campaign since August 2008. In February 2009, a strong gamma-ray flare was accompanied by an optical polarization swing. Two interpretations of this event have been proposed: a blob propagating on a curved trajectory at a few-pc scale, in the region dominated by infrared emission from the dusty torus (IR); and a stationary pattern in a precessing jet in the region dominated by broad emission lines (BEL) [1].

Multiwavelength light curves for the first 2 years of the campaign (2008-2010) and several spectral energy distributions (SEDs) are presented on the poster by Hayashida et al. Here, we model 3 SEDs of unprecedented spectral coverage, thanks to the data from the Spitzer IRS and MIPS instruments: the highest gamma-ray state 'Period D' (MJD 54880-5; Feb 2009), following it state 'Period E' (MJD 54897-900; Mar 2009) and low state 'Period A' (MJD 54682-728; Aug 2008).

MODELING THE BROAD-BAND EMISSION

We fit the SEDs with one-zone leptonic models [2]. The distribution of external radiation is fixed and related to the accretion disk luminosity $L_{\rm d} \simeq 2 \times 10^{45} {\rm erg\,s^{-1}}$. Assuming covering factors $\xi_{\rm BEL} \sim \xi_{\rm IR} \sim 0.1$, the characteristic radii are $r_{\rm BEL} \sim 0.045$ pc and $r_{\rm IR} \sim 1.1$ pc [3]. Energy densities within those radii are $u_{\rm BEL} \sim 0.03$ erg cm^{-3} and $u_{\rm IR} \sim 5.2 \times 10^{-5}$ erg cm^{-3}, outside they decay like $r^{-\beta}$ with $\beta_{\rm BEL} = 3$ and $\beta_{\rm IR} = 4$. Magnetic field strength scales like r^{-1}. The source located at distance r has radius $R = r\theta_{\rm j}$, where $\theta_{\rm j} = 1/\Gamma_{\rm j}$ is the jet opening angle and $\Gamma_{\rm j}$ is the jet Lorentz factor. Electrons are injected with a doubly-broken power-law distribution.

Particularly interesting feature of the Period D SED is a mid-IR break measured by Spitzer/MIPS. The spectral index measured between 70 μm and 160 μm is $\alpha \sim 0.36$. In the ERCIR model it requires an additional break in the electron distribution. In the ERCBEL model, with much more compact emitting region, this break can be explained with the synchrotron self-absorption (SSA). Another feature is the X-ray flux, which shows very little variability during the gamma-ray/optical flare. We treat the X-ray spectrum as an upper limit for SSC and ERC components at periods D and E. It is fitted only in the ERCIR model for Period A.

BLOB PROPAGATION SCENARIO

Polarization swing detected by the Kanata Telescope can be explained by a source propagating on a curved trajectory. A simple model for time dependence of the polarization degree (PD), the polarization angle (PA) and the total flux was proposed by [4]. In Figure 3, we additionally plot the viewing angle $\theta_{\rm obs}$. The predicted values for periods D and E are $\sim 1.5°$ and $\sim 2.4°$, respectively.

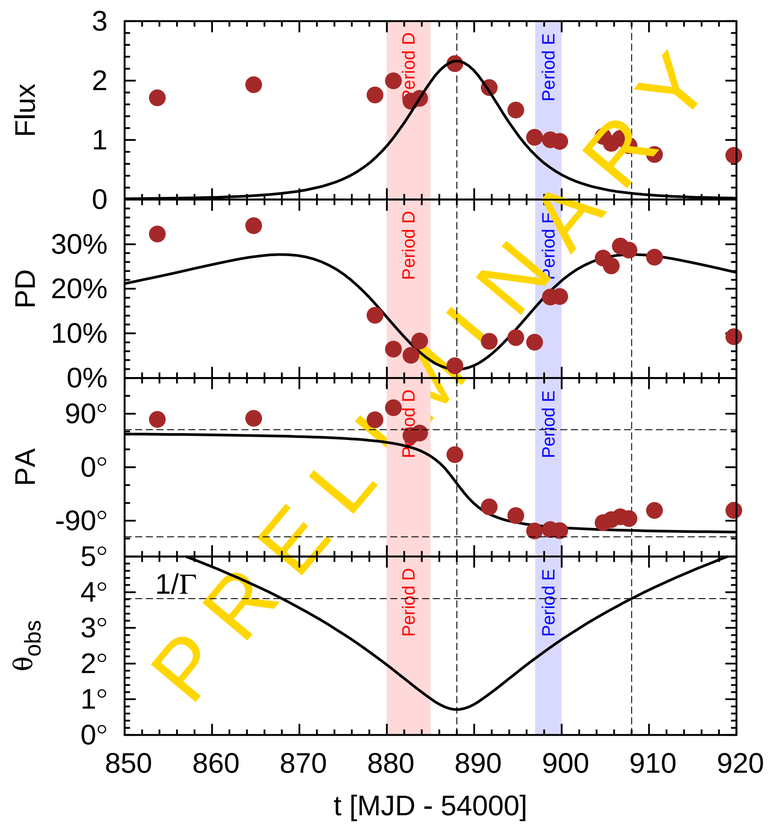

Figure 3: Polarization swing model from [4] compared with the Kanata V-band polarimetric measurements (brown points). From top to bottom: total flux, polarization degree, polarization angle and viewing angle. Periods D and E are indicated with red and blue stripes, respectively.

In Figure 1, we present models D1 and E1, fitted to SEDs at periods D and E, respectively. Model parameters are listed in Table 1. In Model D1, the source is located at $r = r_{\rm IR}$ and in Model E1 at distance larger by $\Gamma_{\rm j}^2 c(\Delta t)$, where $\Delta t \sim 15$ d is the time elapsed between periods D and E. Since the gamma-ray flux decreased by a larger factor than the synchrotron flux, we adopted a steep distribution of the infrared radiation energy density. The Spitzer/MIPS break is explained by the sharp electron break at $\gamma_{\rm br,1} = 800$.

TWO SYNCHROTRON COMPONENTS

In Figure 2, we present Model D2 fitted to SED at Period D with the source located at $r = r_{\rm BEL}$. We adopted a larger Lorentz factor in order to suppress the SSC component. The magnetic field strength, scaled to the same distance, is almost the same as for Model D1. The SSA characteristic wavelength is ~ 100 μm, compatible with the Spitzer/MIPS break. We also show Model A2 fitted to Period A SED, located at the same distance as Model E1. We are able to fit the Spitzer/IRS spectrum, optical/UV, X-ray and gamma-ray data with a singly-broken power-law electron distribution. This indicates that the low-energy SED component of 3C 279 consists of two synchrotron components produced at different distances, as discussed in the case of 3C 454.3 by [5].

Table 1: Comparison of the model parameters.

Model	D1	E1	D2	A2
ext. rad.	IR	IR	BEL	IR
r [pc]	1.1	3.9	0.045	3.9
R [pc]	0.07	0.26	0.0023	0.19
$\Gamma_{\rm j}$	15	15	20	20
$\theta_{\rm j}$ [°]	3.8	3.8	2.9	2.9
$\theta_{\rm obs}$ [°]	1.5	2.4	1.7	1.7
B'(1 pc) [G]	0.14	0.14	0.15	0.15
$\gamma_{\rm br1}$	800	800	170	440
$\gamma_{\rm br2}$	6500	5000	1000	–
p_1	1	1	1	2.2
p_2	2.5	2.6	2.4	3.4
p_3	6	4.2	7	3.4

REFERENCES

[1] Abdo, A. A., et al., 2010, Nature, 463, 919

[2] Moderski, R., Sikora, M., & Błażejowski, M., 2003, A&A, 406, 855

[3] Sikora, M., Stawarz, Ł., Moderski, R., Nalewajko, K., & Madejski, G. M., 2009, ApJ, 704, 38

[4] Nalewajko, K., 2010, IJMPD, 19, 701

[5] Ogle, P. M., Wehrle, A. E., Balonek, T., & Gurwell, M. A., 2010, arXiv:1003.3642